Functional Ecology
December 2021, Volume 35 Issue 12 Pages 2691-2706
https://doi.org/10.1111/1365-2435.13939
https://archimer.ifremer.fr/doc/00733/84480/

Weather and topography regulate the benefit of a conditionally helpful parasite

Monsinjon Jonathan [1, *], McQuaid Christopher D. [1], Nicastro Katy R. [1, 2, 3], Seuront Laurent [1, 2, 3, 4], Oróstica Mauricio H. [1], Zardi Gerardo I. [1]

[1] Department of Zoology and Entomology Rhodes University Grahamstown, South Africa
[2] CCMAR, CIMAR Associated Laboratory University of Algarve Faro, Portugal
[3] Laboratoire d'Océanologie et de Géosciences Univ. Lille CNR SUniv. Littoral Côte d'Opale UMR 8187 LOG Lille ,France
[4] Department of Marine Resources and Energy Tokyo University of Marine Science and Technology Tokyo ,Japan

* Corresponding author : Jonathan Monsinjon, email address : jonathan.monsinjon@gmail.com

Abstract :

1. Heat-induced mass mortalities involving ecosystem engineers may have long-lasting detrimental effects at the community level, eliminating the ecosystem services they provide.

2. Intertidal mussels are ecologically and economically valuable with some populations facing unprecedented heat-induced mass mortalities. Critically, mussels are also frequently infested by endolithic parasites that modify shell albedo, hence reducing overheating and mortality rates under heat stress.

3. Using a biophysical model, we explored the topographical and meteorological conditions under which endolithically driven thermal buffering becomes critical to survival. Based on meteorological data from a global climate analysis, we modelled body temperatures of infested and non-infested mussels over the last decade (2010–2020) at nine sites spread across c. 20° of latitude.

4. We show that thermal buffering is enhanced where and when heat stress is greatest, that is, on sun-exposed surfaces under high solar radiation and high air temperature.

5. These results suggest that new co-evolutionary pathways are likely to open for these symbiotic organisms as climate continues to change, potentially tipping the balance of the relationship from a parasitic to a more mutualistic one. However, endolithically driven reductions in body temperatures can also occur at or below optimal temperatures, thereby reducing the host's metabolic rates and making the interplay of positive and negative effects complex.

6. In parallel, we hindcasted body temperatures using empirical data from nearby weather stations and found that predictions were very similar with those obtained from two global climate reanalyses (i.e. NCEP-DOE Reanalysis 2 and ECMWF Reanalysis v5).

7. This result holds great promise for modelling the distribution of terrestrial ectotherms at ecologically relevant spatiotemporal scales, as it suggests we can reasonably bypass the practical issues associated with weather stations. For intertidal ectotherms, however, the challenge will be incorporating body temperatures over the full tidal cycle.

Keywords : biophysics, ectotherm, heatwave, microhabitat, mussel, mutualism, symbiotic relationship, temperature

Introduction

Heat-induced mass mortalities are becoming more frequent, longer and more severe in both terrestrial (Meehl & Tebaldi 2004) and marine (Di Lorenzo & Mantua 2016; Oliver *et al.* 2018) environments as climate warming progresses. Heat-related mass mortalities have affected a wide variety of taxa including birds (McKechnie & Wolf 2010), mammals (Welbergen *et al.* 2008; Pruvot *et al.* 2019), kelps (Smale 2020), corals (Hughes *et al.* 2017; Le Nohaïc *et al.* 2017), and mussels (Harley 2008; Seuront *et al.* 2019). Such mass mortality events have potentially dramatic cascading effects when they involve ecosystem engineers that provide the biogenic habitat that supports high biodiversity (Smale *et al.* 2019).

Invertebrate body temperatures largely depend on environmental drivers, mediated by body size, shape, positioning, and behaviour, plus intrinsic physical properties (Porter & Gates 1969; Helmuth 1998; Nicastro *et al.* 2012) that are potentially altered by parasitism (Zardi *et al.* 2016; Gehman & Harley 2019). Many marine invertebrates are infested by endolithic fungi, algae or cyanobacteria that bore into their hosts' outer layer and alter their physiology, colour, and morphology (Kaehler 1999; Golubic, Radtke & Campion-Alsumard 2005; Zardi *et al.* 2009; Gleason *et al.* 2017). This is the case for intertidal mussels, which are critical ecosystem engineers (Arribas *et al.* 2014). In these species, endolithic microbes can cause considerable shell damage, reducing scope for growth by increasing metabolic maintenance costs (Ndhlovu, McQuaid & Monaco 2020), eventually leading to host death through shell collapse (Kaehler & McQuaid 1999). During extreme warming events, however, this symbiotic association can become advantageous (Zardi *et al.* 2016; Gehman & Harley 2019; Zardi *et al.* 2021) as discolouration of the shell caused by endolithic activity enhances solar reflectivity so that infested mussels can be 5°C cooler than non-infested

60 individuals, potentially increasing host survival rates during heat waves (Zardi *et al.* 2016;
61 Gehman & Harley 2019).

62 Because the balance between positive and negative effects in host-parasite systems
63 can be context-dependent (e.g., Duncan *et al.* 2010; Bates *et al.* 2011; MacLeod & Poulin
64 2016), we can expect it to change over space and time. To address this in the context of the
65 mussel-endolith system, we identified the topographical and meteorological conditions
66 under which endolithic microbes effectively reduce exposure to heat stress. To achieve this,
67 we predicted the body temperature of non-infested ($Tb_{non\text{-}infested}$) and infested ($Tb_{infested}$)
68 mussels under a range of topographic orientations (i.e., combinations of aspect and
69 inclination angle of the attachment surface) using a biophysical model. To ensure that a
70 wide range of environmental conditions, including extreme weather events, was covered,
71 we reconstructed mussel body temperatures over the last decade (2010-2020) at nine sites
72 spread across ca. 20° of latitude along the north Atlantic coast (Fig. 1, see Table S1 in
73 Supporting Information). Ideally, one would use empirical data from local weather stations
74 to model body temperatures. However, such data are typically scarce, discontinuous, or
75 simply not available during the full extent of the study period. To overcome these practical
76 issues, we used environmental data from a global climate reanalysis. We assessed the
77 validity of this approach by comparing body temperatures reconstructed using data from
78 nearby weather stations and body temperatures recorded *in-situ* with biomimetic sensors
79 (thereafter referred to as "robomussels" following Judge, Choi & Helmuth 2018). Then, we
80 evaluated endolithically-driven thermal buffering by calculating the temperature difference
81 between non-infested and infested mussels ($Tb_{non\text{-}infested} - Tb_{infested}$), categorizing these
82 differences into two levels of thermal buffering: (1) neutral ($Tb_{non\text{-}infested} \approx Tb_{infested}$) and (2)
83 positive ($Tb_{infested} < Tb_{non\text{-}infested}$). Additionally, we calculated the time spent over two critical

thermal thresholds to assess under what circumstances endolithically-driven thermal buffering is sufficient to spare infested mussels from heat-related stress or death.

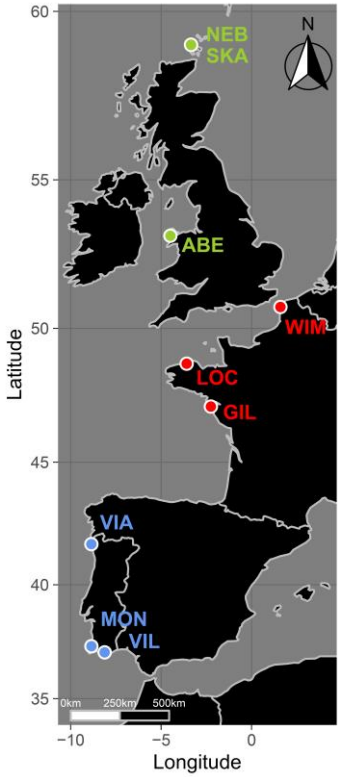

Figure 1. Location of study sites. Mussel body temperatures were predicted for several sites in the United Kingdom (green), France (red), and Portugal (blue). Abbreviations: Nebogeo (NEB), Bay of Skaill (SKA), Aberffraw (ABE), Wimereux (WIM), Locquémeau (LOC), Pointe Saint-Gildas (GIL), Viana do Castelo (VIA), Monte Clerigo (MON), Vilamoura (VIL).

Material and Methods

Biophysical model

We modelled mussel body temperature using the microclimate model implemented in the R package NicheMapR v. 3.0.0 (Porter *et al.* 1973; Kearney & Porter 2017; Kearney 2021) with R v. 4.0.4 (R Core Team 2021). The model computes hourly temperatures at 10 user-specified depths based on the physical first principles of heat exchange (i.e., radiation, convection, conduction, and evaporation) and allows the setting of different types of layers. We set two types of layers: a "mussel" layer for the first 5 cm and a "rock" layer below. For the first layer, we used thermal properties (thermal conductivity = 0.5681 $W.m^{-1}K^{-1}$, specific heat capacity = 3496.3 $J.kg^{-1}K^{-1}$) derived from experiments on *Perna canaliculus* (Mateparae 2003) and other physical properties (density = 1.086 $g.m^{-3}$, water content = 95%) derived from experiments on *Mytilus edulis* and *Mytilus trossulus* (Harbach & Palm 2018). For the second layer, we used thermal properties of a type of granite with high porosity in saturated conditions (thermal conductivity = 2.99 $W.m^{-1}K^{-1}$, specific heat capacity = 800 $J.kg^{-1}K^{-1}$) derived from engineering geology studies (Cho, S. Kwon & Choi 2009; Cho & Kwon 2010) and other physical properties (density = 2.7 $g.m^{-3}$, water content = 34%) derived from measurements on weathered granite (Kwon *et al.* 2011; Rouxel *et al.* 2012). Microclimate was computed at 5-cm height and temperature predictions were obtained at 2.5-cm depth, representing internal body temperatures (Tb) at the scale of a large mussel bed. Based on reflectance measurements for *Mytilus californianus* (Gehman & Harley 2019), we set reflectivity at 0.161 and 0.245, respectively for non-infested (darker) and infested (paler) mussels, to compute $Tb_{non\text{-}infested}$ and $Tb_{infested}$. We calculated these values from 350 nm to 1100 nm based on reflectance spectra of eroded and non-eroded shells (previously digitized from Fig. 4A in Gehman & Harley 2019) and the ASTM G-173 standard irradiance spectrum for dry air derived from SMARTs v. 2.9.2 (Gueymard 2001) using the formula in Smith *et al.*

(2016). NicheMapR allows the user to predict temperatures of the substratum (or the organism) during periods of submergence, calculating heat balance via conduction and convection only (see parameter 'shore' in NicheMapR's help). We selected this option whenever mussels were expected to be submerged (i.e., when tidal levels were higher than the mussels' height on the shore). To distinguish between periods of submergence and aerial exposure, we calculated the Effective Shore Level (ESL), an estimate of intertidal height using temperature profiles and tidal heights (Harley & Helmuth 2003; Gilman *et al.* 2006). The method uses sudden drops in logger temperatures and the corresponding tidal height at this time to estimate when robomussels are first immersed by the returning tide. We obtained hourly tidal predictions (using the XTide software; https://flaterco.com/xtide/) for nearby maritime ports (Table S2) and interpolated tidal levels at 30-min intervals (using na.approx function from the R package zoo; Zeileis & Grothendieck 2005) to match the time at which robomussels were set to record temperature (see Zardi *et al.* 2021). We retrieved all tidal levels that were associated with a temperature drop of > 8°C in 30 min during incoming tides. This corresponds to a drop of 5.33°C in 20 min, ensuring the reliability of ESL estimates and maximising the probability of correctly identifying the effects of tidal emersion (Gilman *et al.* 2006). For each study site, we then calculated the mean ESL (± standard deviation, SD) using temperature data from all robomussels pooled together (Table S3). Finally, we ran the model under most possible topographic orientations by varying the inclination angle ('slope' from 0° to 90° every 10°) and the direction that the surface faces ('aspect' in degrees North from 0° to 350° every 10°). We assumed moist air conditions with no shade, no moisture throughout the substratum, no vegetation and no organic matter or snow cover over the mussel layer. The other parameters were left as

default (see settings in NicheMapR's help for the following functions: microclimate, micro_ncep and micro_era5).

Meteorological data

To predict mussel body temperatures during aerial exposure, we drove the NicheMapR microclimate model using three sources of meteorological data. Air temperature, wind speed, solar radiation, relative humidity, precipitation, and cloud cover were obtained from: (i) nearby weather stations (Table S4), (ii) the NCEP-DOE Reanalysis 2 (Kanamitsu *et al.* 2002) hereafter referred to as NCEP, and (iii) the ECMWF Reanalysis v5 (Hersbach *et al.* 2019) hereafter referred to as ERA5. Weather station observations in the United Kingdom (Met Office 2019a; Met Office 2019b; Met Office 2019c), France and Portugal were provided by the Centre for Environmental Data Analysis (CEDA; http://data.ceda.ac.uk/badc/ukmo-midas-open/data/), Météo-France (https://donneespubliques.meteofrance.fr/) and Instituto Portugês do Mar e da Atmosfera (IPMA; https://www.ipma.pt/en/otempo/obs.superficie/), respectively. Note that cloud cover was not available from weather stations and was therefore calculated from the ratio of hourly clear sky solar radiation (previously computed using NicheMapR's microclimate function) compared to the observed hourly global solar radiation measured by weather stations (Kearney *et al.* 2014; Kearney & Porter 2017). In addition, wind speed was measured at 10-metre height and downscaled to a height of 2 m using the formula in Kearney *et al.* (2014) to match the model's reference height. We computed aerosol attenuation using a global aerosol data set (Koepke *et al.* 1997) to account for scatter from atmospheric particles (Kearney & Porter 2017). Occasional missing data (see Fig. S1 in Supporting Information) were linearly interpolated using na.approx

function from the R package zoo (Zeileis & Grothendieck 2005). For three of our sites, we could not predict mussel body temperatures using observations from weather stations because solar radiation data were not available (Fig. S1, Table S4). Alternatively, NCEP and ERA5 global climate reanalyses provide all required data on a continuous time scale from 1979 onward (6-hourly and hourly, respectively) at different spatial resolution (2.5° × 2.5°and 0.25° × 0.25°, respectively). To compute mussel body temperatures from NCEP data, we used NicheMapR's micro_ncep function, which integrates some functions of the R packages microclima (Maclean, Mosedale & Bennie 2018; Mosedale, Bennie & Duffy 2021), elevatr (Hollister 2020), rnooa (Chamberlain 2021), and RNCEP (Kemp *et al.* 2012) to compute mesoclimate effects such as elevation-associated lapse rates, wind sheltering, coastal influences and cold air drainage (but see Kearney *et al.* 2020 for details). We used a similar function (micro_era5), which integrates a function of the R package mcera5 (Duffy in prep), to compute mussel body temperatures from ERA5 data. Here, we tested whether accounting for coastal influence due to exposure to the sea improved estimates of mussel body temperature during aerial exposure. To do so, we ran micro_ncep and micro_era5 with and without the coastal influence option and compared the output based on goodness-of-fit metrics (see section below). To predict mussel body temperatures during submergence, we drove the model using hourly sea surface temperatures extracted at our study sites from ERA5.

Model validation

To validate the approach and select the most suited source of meteorological data, we compared our predictions of $Tb_{non\text{-}infested}$ and $Tb_{infested}$ with temperature data recorded *in-situ*

using robomussels (Judge, Choi & Helmuth 2018) previously deployed at our nine study sites in summer 2017 and 2018 (Fig. S2 and Table S1, but see Zardi *et al.* 2021 for details). At each site, three to six pairs of robomussels (one infested and one non-infested using shells of *Mytilus galloprovincialis*) were deployed within the mid mussel zone on a relatively flat surface (< 20°) and equidistant from each other (ca. 10 cm). In the original study, Zardi *et al.* (2021) did not measure the exact slope and aspect of the surface where robomussels were placed. Therefore, we chose to infer their topographic orientation by searching for the combination of aspect and inclination angle that best described temperatures recorded *in-situ* by robomussels during aerial exposure. To do so, we computed $Tb_{non\text{-}infested}$ and $Tb_{infested}$ for three possible inclination angles (0°, 10°, 20°) and every possible aspect (from 0° to 350° every 10°), and we selected the topographic orientation individually for each pair of robomussels based on the lowest Root Mean Square Error (RMSE). We also calculated Pearson's correlation coefficient as an additional goodness-of-fit metric, with higher correlation coefficients indicative of a better fit between observations and predictions. We assessed the validity of our approach to predict mussel body temperatures during periods of submergence using the same metrics. Note, however, that the method used here to distinguish between periods of aerial exposure and submergence (i.e., when tidal levels are, respectively, lower or higher than the estimated elevation of mussels on the shore) may introduce some bias. In fact, the ESL is not meant to be fixed. Instead, ESLs can vary between tidal cycles due to surge and wave exposure (Gilman *et al.* 2006). To overcome this, we followed Lathlean, Ayre and Minchinton (2011) in ensuring that temperature data were correctly attributed to periods of aerial exposure or submergence by applying a buffer zone (mean ESL ± 0.3 m). We excluded all data that fell within this buffer zone when calculating goodness-of-fit metrics.

Thermal buffering

Using meteorological data from one of the global climate reanalyses, we reconstructed $Tb_{non\text{-}infested}$ and $Tb_{infested}$ from 2010-01-01 to 2020-01-01 for a wide range of topographic orientations at our nine study sites. Using these temperature time series, we evaluated endolithically-driven thermal buffering by calculating the proportion of time spent within two categories of thermal buffering, one defined as neutral ($Tb_{non\text{-}infested} \approx Tb_{infested}$) and the other as positive ($Tb_{non\text{-}infested} < Tb_{infested}$). We chose a 0.5°C cut-off to distinguish between these two categories because such a difference in body temperature entails less than 50% difference in survival when approaching critical thermal limits (Seuront *et al.* 2019; Ndhlovu, McQuaid & Monaco 2020). In other words, thermal buffering is considered neutral if the absolute difference between $Tb_{non\text{-}infested}$ and $Tb_{infested}$ is ≤ 0.5°C or positive if the difference is > 0.5°C. We used these categories to identify where (topographic orientation) and when (time of day) thermal buffering is enhanced. On the other hand, we aimed to identify the meteorological conditions associated with the lowest and highest differences between $Tb_{non\text{-}infested}$ and $Tb_{infested}$. To do so, we used body temperatures predicted for mussels on a horizontal surface during aerial exposure and retrieved the data on solar radiation, wind speed, air temperature, and relative humidity (downscaled at 5-cm height with NicheMapR). In this case, we categorized endolithically-driven temperature differences as follows: [minimum, 5th percentile] and [95th percentile, maximum], respectively for the lowest and highest ranges of body temperature differences.

Commenté [JM1]: Error: $Tb_{infested} < Tb_{non\text{-}infested}$

Commenté [JM2]: within intervals

Critical thermal limits

To test whether the change in shell reflectance caused by endoliths provides an effective defence against heat stress, we calculated the time spent over two critical thermal thresholds independently for non-infested and infested mussels. The lethal temperature at which approximately half of individuals are expected to die (LT_{50}) lies between 35°C and 38°C based on experiments on *Mytilus californianus* and *Mytilus galloprovincialis* (Denny *et al.* 2011; Sorte *et al.* 2019) and the lethal temperature at which almost all individuals are expected to die (LT_{100}) is 41°C based on experiments on *Mytilus californianus* (Denny *et al.* 2011). Therefore, we chose LT_{50} = 38°C and LT_{100} = 41°C as critical thermal limits for survival. On the other hand, it is possible that endolithically-driven thermal buffering reduces body temperatures even within the optimal range of thermal performances, thus adding a potential cost of endolith infestation if $Tb_{infested}$ falls below optimal temperatures, reducing metabolic rate. To assess this, we retrieved $Tb_{non\text{-}infested}$ and $Tb_{infested}$ expected in sun-sheltered and sun-exposed habitats (North-facing at 90° inclination and South-facing at 20° inclination, respectively) and compared body temperatures with lethal and optimal thermal ranges. Based on metabolic rate experiments, optimal thermal performances occur roughly between 22°C and 32°C for *M. californianus* (Monaco, Wethey & Helmuth 2016) and the optimal body temperature (Tb_{opt}) lies around 30°C for *M. galloprovincialis* (Monaco & McQuaid 2018).

Results

Model validation

Overall, using meteorological data from either nearby weather stations or global climate reanalyses (NCEP and ERA5) yielded very similar results (Fig. 2, Table S5), albeit the mean

RMSE across all sites was slightly lower when using weather stations observations: RMSE < 3°C (Fig. 2a) vs RMSE ≈ 3°C (Fig. 2c,e,g,i). Note, however, that the mean RMSE and correlation coefficient calculated across all sites for weather station data (Fig. 2a-b) are not directly comparable to those calculated for climate reanalyses (Fig. 2c-j) because they do not include predictions from three sites (LOC, GIL, and VIA; Fig. 2a-b). At the site level, the fit was sometimes slightly better when using NCEP or ERA5 data instead of weather station observations (Fig. 2, Table S5). Some RMSEs were lower for ABE, MON and VIL (26% of our dataset) when using NCEP data, and for WIM and VIL (16% of our dataset) when using ERA5 data (Table S5). Some correlation coefficients were higher for MON and VIL (13% of our dataset) when using NCEP data, and for SKA, ABE, WIM, MON and VIL (32% of our dataset) when using ERA5 data (Table S5). On the other hand, accounting for coastal influences did not improve body temperature predictions during aerial exposure when using either NCEP (Fig. 2e-f) or ERA5 (Fig. 2i-j) data. During submergence, the fit was reasonably good (i.e., RMSE ≤ 3°C and correlation coefficient ≥ 0.5) for WIM only (Table S5). Given that the approaches tested here yielded similar outcomes (Fig. 2, Table S5), we selected the less computationally demanding one (i.e., NCEP with no coastal effects) to predict long-term mussel body temperatures and explore the effect of topographic orientation. With a few exceptions, this approach allowed us to reconstruct body temperature trajectories with reasonable accuracy (Fig. S2). During emergence, high robomussel temperatures were slightly underestimated and low temperatures slightly overestimated (Fig. S3), except for one pair of robomussels at one site (third pair of robomussel at LOC) which showed the worst fit. During submersion, high robomussel temperatures were strongly overestimated and low robomussel temperatures strongly underestimated (Fig. S3), with a few exceptions

Commenté [JM3]: weather station observations

279 showing the opposite relationship (NEB, SKA, and VIA) or a closer accordance between

280 predicted and recorded temperatures (MON, VIL, and the third pair of robomussel at LOC).

281

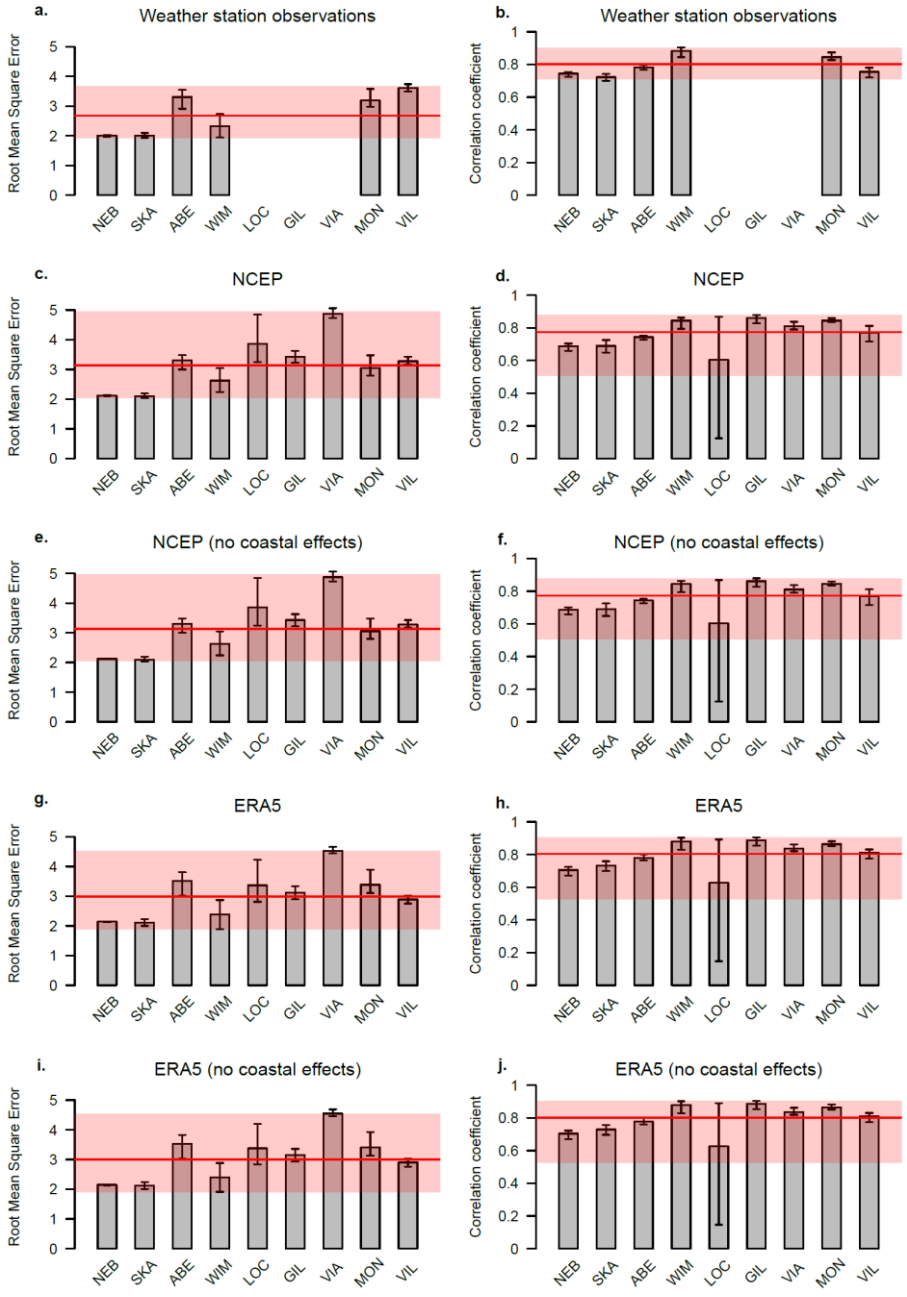
a.
Weather station observations
Root Mean Square Error
b.
Weather station observations
Correlation coefficient
c.
NCEP
Root Mean Square Error
d.
NCEP
Correlation coefficient
e.
NCEP (no coastal effects)
Root Mean Square Error
f.
NCEP (no coastal effects)
Correlation coefficient
g.
ERA5
Root Mean Square Error
h.
ERA5
Correlation coefficient
i.
ERA5 (no coastal effects)
Root Mean Square Error
j.
ERA5 (no coastal effects)
Correlation coefficient
NEB
SKA
ABE
WIM
LOC
GIL
VIA
MON
VIL

282

Figure 2. Model validation. Goodness-of-fit metrics for the prediction of mussel body temperature (Tb) during aerial exposure using either weather station observations (**a**, **b**) or global climate reanalyses: NCEP with and without coastal influence (respectively **c**, **d**, and **e**, **f**) and ERA5 with and without coastal influence (respectively **g**, **h**, and **i**, **j**). Histograms represent mean RMSEs (left panels) and mean correlation coefficients (right panels) for every site, and error bars are 2.5th and 97.5th percentiles. Red lines represent the mean across all sites, and red shaded areas are 2.5th and 97.5th percentiles. Predictions of Tb were compared with temperatures recorded *in-situ* using pairs of robomussels (i.e., biomimetic sensors built with shells of either infested or non-infested mussels). Tb was predicted for specific combinations of aspect and inclination angle for each pair of robomussels (Table S5). Tb was not predicted for LOC, GIL, and VIA because solar radiation was not available from nearby weather stations. From left to right, sites are given north to south (for abbreviations: see Fig. 1).

Under what topographic orientations is thermal buffering enhanced?

Thermal buffering was essentially neutral under most topographic orientations (Fig. 3a,c,e). Thermal buffering was, however, sometimes positive (roughly within 5-25% of the time for most locations; Fig. 3b,d,f) on horizontal and inclined surfaces with angles increasing from 10° up to 90° as the aspect shifts from 90° to 180° (i.e., clockwise from East to South) or from 270° to 180° (i.e., anticlockwise from West to South). This general pattern whereby endolithically-driven thermal buffering can be positive on sun-exposed surfaces was consistent across study sites, albeit with important variations in the maximum proportion of time spent under each category of thermal buffering (Fig. 3, Fig. S4). For instance, thermal

306 buffering was almost never positive at two high-latitude sites (NEB and SKA; Fig. S4) but also
307 rarely positive (roughly within 5-10% of the time) at two low-latitude sites (MON and VIL;
308 Fig. S4). Under the same range of topographic orientations, and especially on South-facing
309 surfaces at 20-30° inclination, thermal buffering was positive up to 35% of the time at two
310 distant sites (LOC and VIA) while it did not exceed 20% of the time at relatively closer sites
311 (e.g., GIL and MON, respectively for comparison with LOC and VIA; Fig. S4).

312 During the day, we can expect thermal buffering to be positive at any time but mostly
313 between 08:00 and 21:00 (i.e., when exposed to sunlight) with a peak in frequency
314 occurring between 12:00 and 14:00 (Fig. 4). At this time of day, thermal buffering was most
315 frequently positive on Southeast- and South-facing surfaces as compared to Northwest- and
316 North-facing ones, albeit the difference was invariably minimal at 20° inclination (Fig. S5a).
317 At 90° inclination, however, thermal buffering was almost never positive on surfaces that
318 are sheltered from sunlight during a large part of the day (i.e., Northwest, North, and
319 Northeast) while it was most frequently positive in other cases (Fig. S5b). In these latter
320 cases, thermal buffering can be positive only between 08:00 and 21:00, with a peak in
321 frequency occurring at different times depending on the aspect (Fig. S5b). In fact, the peak
322 occurred at 11:00 and 12:00 on surfaces exposed to morning sunlight and shifted
323 progressively to 15:00 and 16:00 on surfaces exposed to afternoon sunlight (Fig. S5b).

324

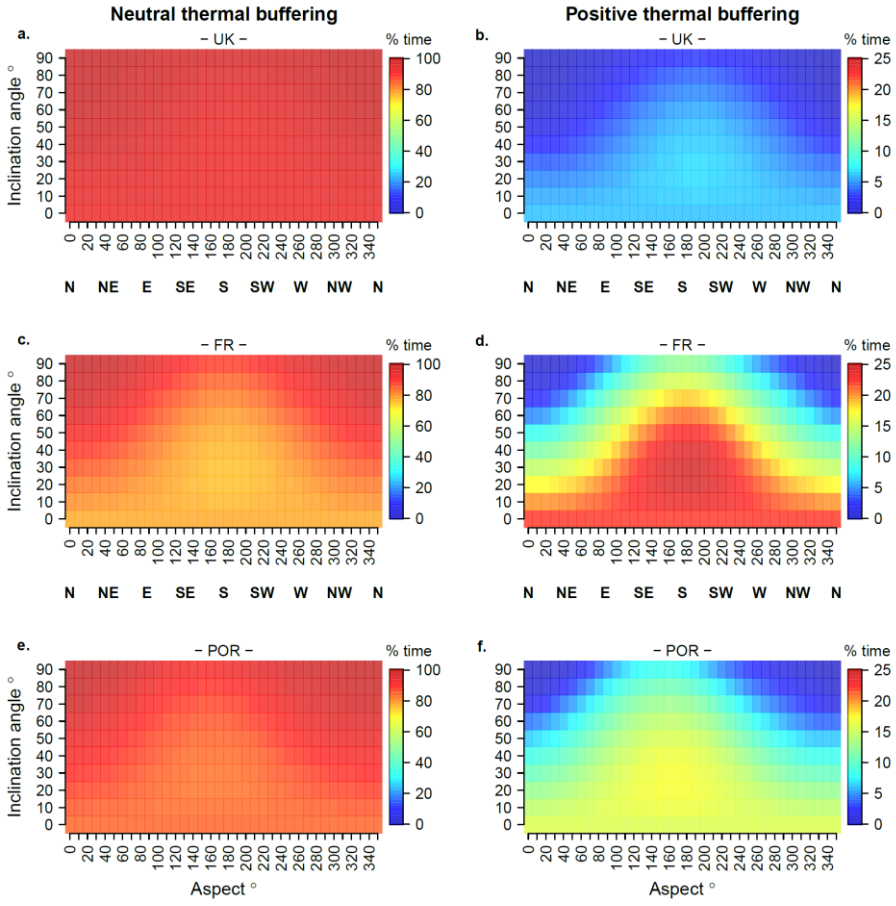

Figure 3. Topographic orientation and endolithically-driven thermal buffering. Proportion of time (% time in colour scale) spent under two categories of thermal buffering: neutral (left panels) if $Tb_{non\text{-}infested} \approx Tb_{infested}$ and positive (right panels) if $Tb_{infested} < Tb_{non\text{-}infested}$ based on body temperatures predicted between 2010-01-01 and 2020-01-01 for sites in the United Kingdom (**a**, **b**), France (**c**, **d**), and Portugal (**e**, **f**). Letters in bold indicate cardinal directions.

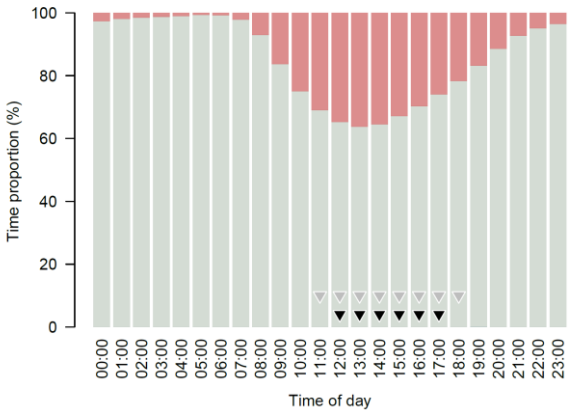

Figure 4. Time of day and endolithically-driven thermal buffering. Colours indicate the proportion of time spent under two categories of thermal buffering: neutral (grey) if $Tb_{non\text{-}infested} \approx Tb_{infested}$ and positive (red) if $Tb_{infested} < Tb_{non\text{-}infested}$ based on body temperatures predicted between 2010-01-01 and 2020-01-01 on a horizontal surface (all study sites pooled together). Triangles indicate the time of day when body temperature exceeded 38°C (grey) or 41°C (black) at least once.

Under what meteorological conditions is thermal buffering enhanced?

Considering a horizontal surface, the lowest differences between $Tb_{non\text{-}infested}$ and $Tb_{infested}$ ranged from -0.52°C to 0.01°C and the highest from 1.36°C to 3.23°C (Fig. 5a). The lowest differences occurred under extremely low solar irradiance, low to high wind speed, low air temperature, and high relative humidity (Fig. 5b-e). Under such conditions, both non-infested and infested mussels experienced similar body temperatures (i.e., $Tb_{non\text{-}infested} = Tb_{infested}$ = 9.34°C ± 3.06°C; mean ± SD). In contrast, the greatest differences between $Tb_{non\text{-}infested}$ and $Tb_{infested}$ occurred under moderate to high solar irradiance, mostly low wind

speed, high air temperature, and moderate relative humidity (Fig. 5b-e). Under these conditions, non-infested mussels were on average warmer ($Tb_{non\text{-}infested}$ = 31.64°C ± 4.37°C) than infested ones ($Tb_{infested}$ = 29.89°C ± 4.14°C).

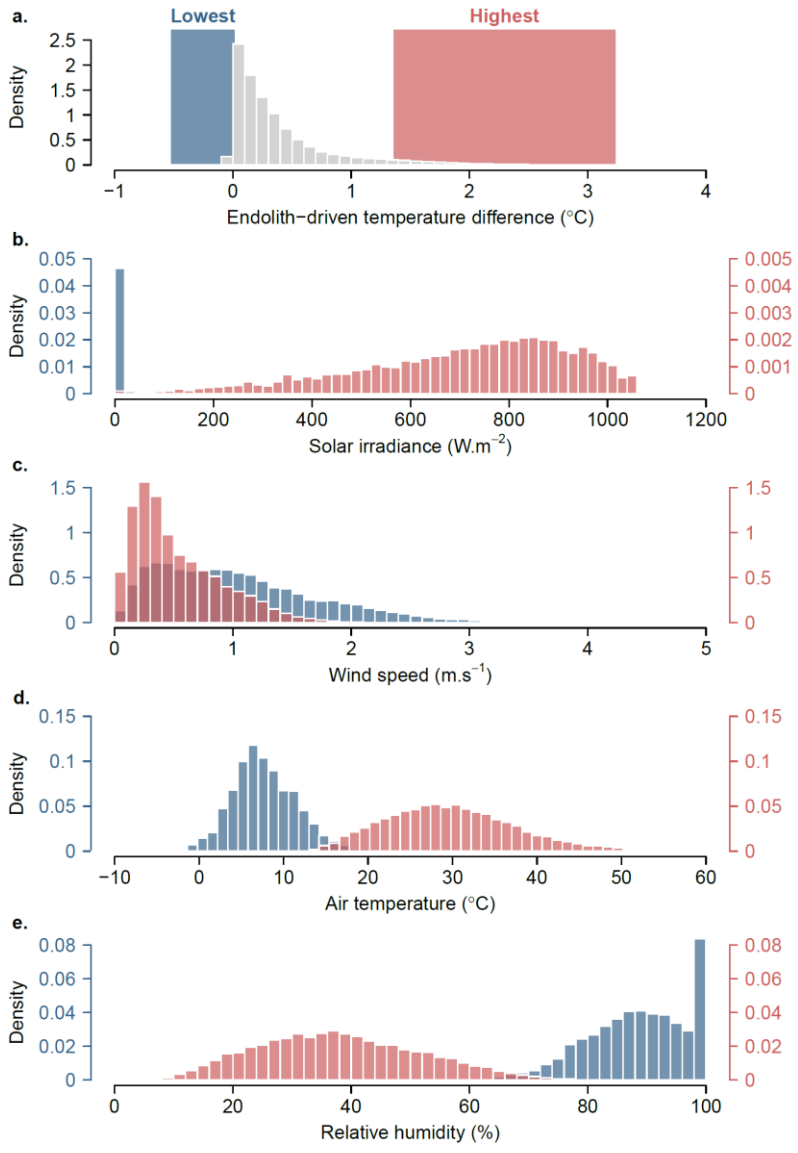

Figure 5. Differences in body temperature and associated meteorological conditions. Distribution of (**a**) differences in body temperature ($Tb_{non\text{-}infested}$ - $Tb_{infested}$) during aerial exposure and considering a horizontal surface (all study sites pooled together), (**b**) solar irradiance, (**c**) wind speed, (**d**) air temperature, and (**e**) relative humidity. Coloured areas in panel **a** encompass the lowest (blue) and highest (red) ranges of differences between $Tb_{non\text{-}infested}$ and $Tb_{infested}$. Colours in the other panels display the distribution of each meteorological variable when $Tb_{non\text{-}infested}$ - $Tb_{infested}$ fell within either the lowest (blue) or the highest (red) range.

Do endoliths effectively protect their host from overheating?

On surfaces sheltered from the sun most of the time (i.e., steep inclination angles and aspects shifting away from the South), neither $Tb_{infested}$ nor $Tb_{non\text{-}infested}$ exceeded 38°C (Fig. 6, Fig. S6). In contrast, on more exposed surfaces, $Tb_{non\text{-}infested}$ often exceeded 38°C while $Tb_{infested}$ remained below this critical threshold. A similar pattern emerged when considering a higher thermal threshold (i.e., 41°C), albeit with a more marked difference between infested and non-infested mussels (Fig. 7, Fig. S7). At sites in the United Kingdom, $Tb_{infested}$ never exceeded 41°C while $Tb_{non\text{-}infested}$ exceeded this threshold for a few hours (Fig. 7a-b) at one site (ABE; Fig. S7). At the other sites in France and Portugal, $Tb_{infested}$ sometimes exceeded 41°C but less often and under a much narrower range of topographic orientations (i.e., essentially South-facing surfaces with a slight inclination) than values for $Tb_{non\text{-}infested}$ (Fig. 7c-f, Fig. S7). On a horizontal surface (or for any aspect with a slight inclination) lethal body temperatures were exceeded between 11:00 and 19:00 (Fig. 4, Fig. S5a). On the other hand, lethal body temperatures were never reached on any vertical surfaces (Fig. S5b). In

376 fact, when considering a fully sun-sheltered surface, where body temperatures never
377 reached any critical threshold, endolithically-driven thermal buffering remained minimal
378 (Fig. 8a). In contrast, when considering a fully sun-exposed surface, endolithically-driven
379 thermal buffering was progressively enhanced while approaching and exceeding lethal
380 temperatures (Fig. 8b). Note that, in such cases, infested mussels could be up to 2°C cooler
381 than non-infested ones while $Tb_{non\text{-}infested}$ was at the lower limit of optimal body
382 temperatures (Fig. 8b).

383

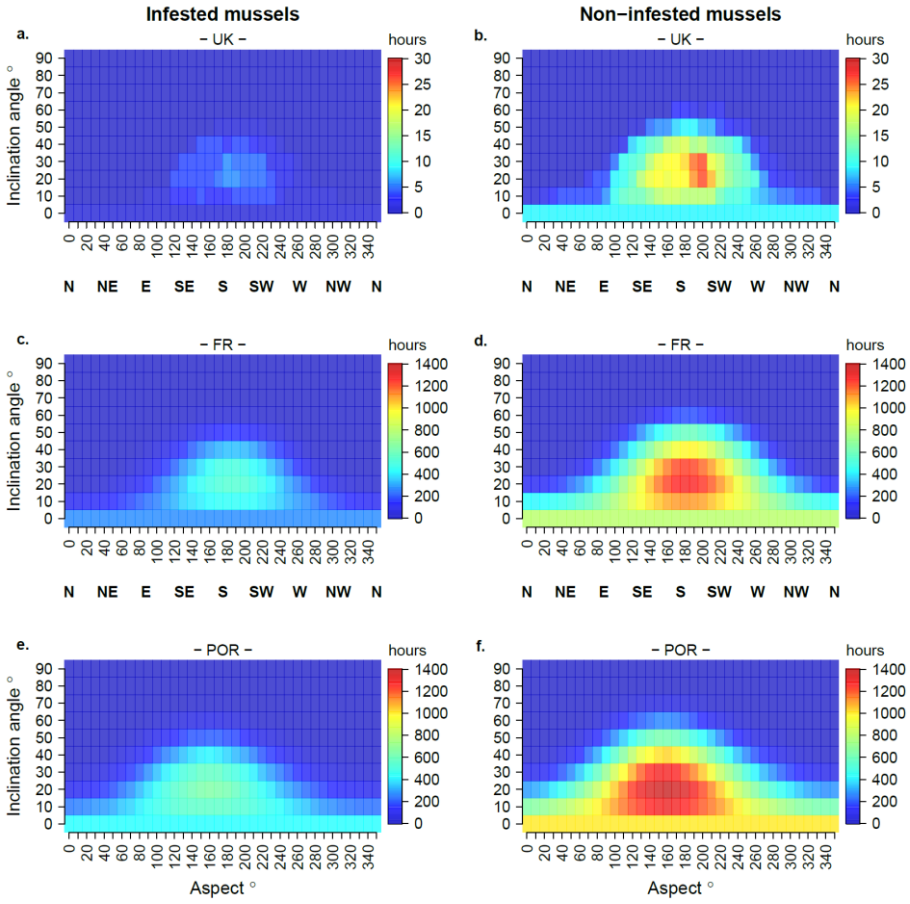

384

385 **Figure 6. Topographic orientation and time spent over 38°C.** Number of hours (in colour

386 scale) spent over 38°C for $Tb_{infested}$ (left panels) and $Tb_{non\text{-}infested}$ (right panels) based on body

387 temperatures predicted between 2010-01-01 and 2020-01-01 for sites in the United

388 Kingdom (**a**, **b**), France (**c**, **d**), and Portugal (**e**, **f**). Letters in bold indicate cardinal directions.

389

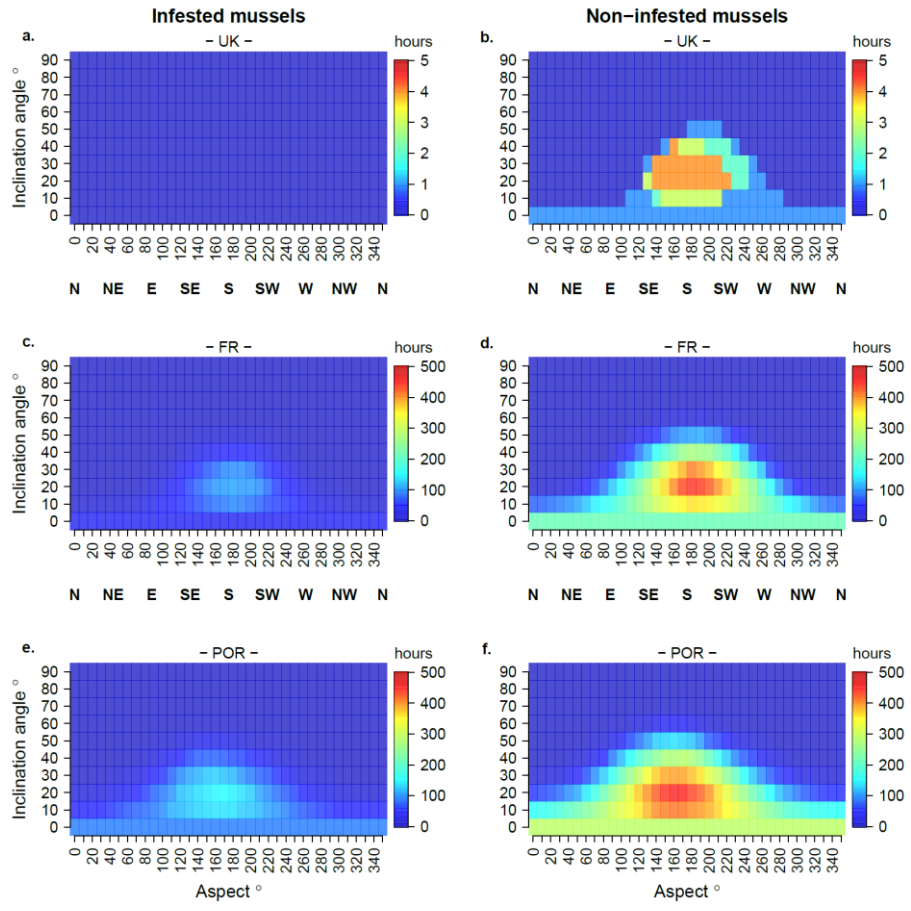

Figure 7. Topographic orientation and time spent over 41°C. Number of hours (in colour scale) spent over 41°C for $Tb_{infested}$ (left panels) and $Tb_{non\text{-}infested}$ (right panels) based on body temperatures predicted between 2010-01-01 and 2020-01-01 for sites in the United Kingdom (**a**, **b**), France (**c**, **d**), and Portugal (**e**, **f**). Letters in bold indicate cardinal directions.

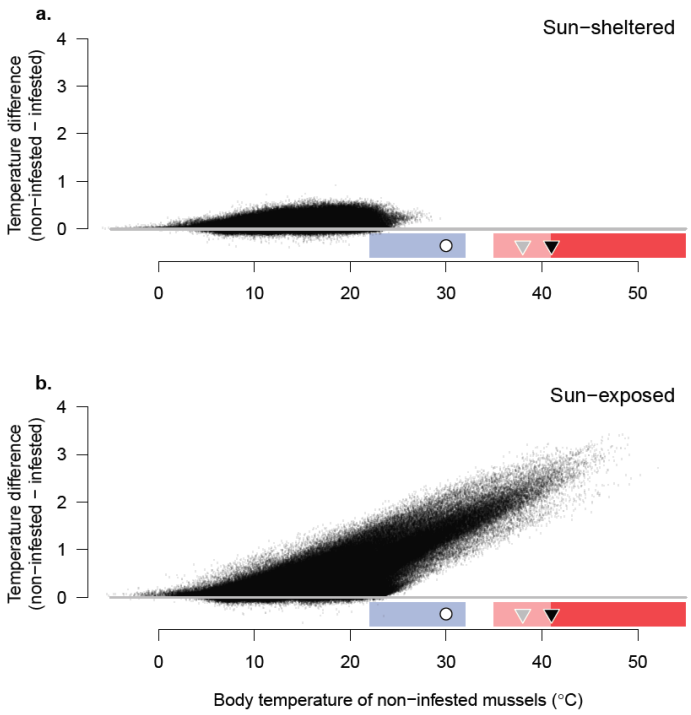

396

397 **Figure 8. Efficiency of endolithically-driven thermal buffering under two distinct**

398 **topographic orientations.** Temperature difference ($Tb_{non\text{-}infested}$ - $Tb_{infested}$) vs $Tb_{non\text{-}infested}$

399 based on body temperatures predicted between 2010-01-01 and 2020-01-01 (all study sites

400 pooled together) on a surface sheltered from the sun, i.e., North-facing at 90° inclination (**a**)

401 and an exposed one, i.e., South-facing at 20° inclination (**b**). Coloured areas cover optimal

402 (blue) and lethal (red) ranges of body temperature (the area in light red covers

403 temperatures at which some individuals may still survive). White circles indicate the optimal

404 temperature (T_{obt}), and grey and black triangles indicate lethal temperatures (LT_{50} and LT_{100},

405 respectively).

406

Discussion

Our study demonstrates that the thermal buffering effect conferred by parasitic endoliths is mostly neutral for most topographic orientations. Thermal buffering is, however, advantageous when heat stress is greatest, that is, on sun-exposed surfaces, between midday and late afternoon, during hot weather, with clear skies and light winds. The context-dependent protection against harmful temperatures can make a difference during heat waves by giving infested mussels a higher chance of survival (Gehman & Harley 2019; Zardi *et al.* 2021). This result is particularly relevant for populations of intertidal mussels, which, like most intertidal ectotherms, live at or near the upper limits of their thermal tolerances (Somero 2010). As climate changes, with an increase in solar radiation due to decreased cloud cover (Schneider, Kaul & Pressel 2019), endolithically-driven thermal buffering could prevent the extirpation of important mussel populations and potentially redirect these partners toward a novel co-evolutionary pathway. Such mutualistic relationships may open new ecological opportunities (Wellborn & Langerhans 2015) as they can allow the host to experience less thermal stress at the hottest edges of their small- and large-scale distributional ranges (i.e., the intertidal zone and biogeographic regions, respectively). Our results further suggest, however, that mussels living in sun-sheltered microhabitats (or during mild weather) are not (or much less) exposed to stressful temperatures, in which case infested mussels are clearly at a competitive disadvantage because they suffer only the costs imposed by endoliths, namely considerable shell damage leading to increased metabolic maintenance costs (Ndhlovu, McQuaid & Monaco 2020) and eventually death through shell collapse (Kaehler & McQuaid 1999).

Modulation of thermal buffering

Under solar radiation, low-reflectance individuals gain heat faster and reach higher equilibrium temperatures than their higher-reflectance counterparts (Porter & Gates 1969), so that one could expect the evolution of light body pigmentation in hot climates (Gibert *et al.* 1998). In climates where it is important to gain solar heat as rapidly as possible in order to maximise the time available for foraging or mate-finding, darker ectothermic animals can show better survival and reproductive success than their paler counterparts (Clusella Trullas, van Wyk & Spotila 2007; Clusella-Trullas *et al.* 2008; Smith *et al.* 2016). However, reflectance also affects the rate of cooling, with dark ectotherms loosing heat faster (Geen & Johnston 2014). All else being equal, the rate of solar heat gain depends on more than just colour (Walsberg, Campbell & King 1978; Walsberg 1983; Turner & Lombard 1990; Helmuth 1998; Umbers, Herberstein & Madin 2013). For instance, the heat budget of small animals is more dependent on convective cooling than radiative heating (Turner & Lombard 1990; Helmuth *et al.* 2011; Umbers, Herberstein & Madin 2013) and this effect can be amplified in dark animals under thin boundary layer conditions (Walsberg, Campbell & King 1978; Walsberg 1983). This explains why non-infested mussels were sometimes slightly cooler than infested ones and reinforces the importance of both wind speed and the microhabitat in thermal buffering (Seabra *et al.* 2011; Zardi *et al.* 2021). In intertidal mussels, orientation relative to the substratum can result in large temperature differences among individuals lying close together; such microscale differences can even exceed seasonal variation depending on whether they are sheltered from the sun (e.g., North-facing vertical surfaces in the northern hemisphere) or exposed to direct sunlight during a large part of the day (Harley 2008; Seabra *et al.* 2011; Choi *et al.* 2019). Here, we show that topographic orientation and exposure to sunlight regulate the thermal buffering effect of endoliths, with infested

454 mussels expected to (i) be more frequently cooler, and (ii) avoid overheating more often
455 than non-infested ones on sun-exposed surfaces (e.g., South-facing at 20° inclination)
456 between roughly midday and late afternoon. These are precisely the times and places when
457 mussels are most likely to be exposed to high air temperatures and direct sunlight, so that
458 non-infested mussels warm up faster and to higher temperatures than infested ones. We
459 predicted that, on a horizontal surface, the lowest differences in body temperature between
460 infested and non-infested mussels would occur under very low solar irradiance and cool air
461 temperature. Such conditions are likely to occur at night or during cloudy days, that is, when
462 overheating is unlikely. Conversely, endolithically-driven thermal buffering is greatest and
463 most likely to enhance survival during heat waves under clear sky conditions, when mussels
464 may come dangerously close to lethal temperatures. Here we show that thermal buffering
465 does indeed allow infested mussels to remain below 38°C or 41°C more often than non-
466 infested ones and under a wider range of topographic orientations, with some variation in
467 the maximum time spent over these critical thresholds across study sites due to differences
468 in latitude but also factors influencing at small scales such as tidal amplitude and time spent
469 under aerial exposure (Helmuth *et al.* 2006). For instance, our predictions of body
470 temperatures suggest that both infested and non-infested mussels never reached 38°C at
471 two sites in the North of the United Kingdom (at least during our study period) while they
472 reached 41°C more than once on sun-exposed surfaces at other sites. This suggests that
473 endolithically-driven thermal buffering does not necessarily provide an advantage at the
474 coldest edges of the large-scale distributional range of mussels (at least for *Mytilus* spp. in
475 our case). It is also important to note that thermal preferences and critical thermal
476 thresholds can vary at different levels, from individuals (e.g., via acclimatization) to
477 populations (e.g., via local adaptation; Sanford & Kelly 2011; Thyrring, Tremblay & Sejr

2019). Here, for a more general approach, we used data obtained from the literature for two distinct species: *Mytilus californianus* and *Mytilus galloprovincialis* (Monaco & McQuaid 2018; Sorte *et al.* 2019). Future studies would be needed to further highlight any potential intraspecific variation by incorporating population-specific and inter-individual variation in critical temperatures.

Balance between parasitism and mutualism

In line with previous studies (Zardi *et al.* 2016; Gehman & Harley 2019), we highlight an example of a symbiotic relationship that switches between parasitism and mutualism, whereby the host mostly suffers from the damage caused by endoliths but sometimes benefits from the thermal buffering they provide. On sun-exposed surfaces in most of our study sites, we predicted that non-infested mussels would have experienced lethal temperatures while infested individuals were exposed less often or not at all to stressful or lethal body temperatures. This should allow infested mussels to show higher fitness and better survival than non-infested individuals in places where body temperatures approach or reach the species' upper thermal tolerances. In other words, endolithic infestation is potentially increasing the width of the realized thermal niche. However, we also showed that the cost of endolithic infestation is not outweighed by any thermal advantage in sun-sheltered microhabitats, and that thermal buffering can sometimes reduce body temperatures when the animals are already within their optimum thermal range. Rocky shores are often topographically complex, and thus provide their inhabitants with a huge diversity of thermal microhabitats (Helmuth *et al.* 2006; Harley 2008; Denny *et al.* 2011; Seabra *et al.* 2011). In such situations, it is unlikely that all infested individuals will exhibit

501 higher fitness than non-infested ones at the same shore level. In turn, in environments
502 where intertidal mussel beds are located on relatively flat reefs, such as along the French
503 coast of the eastern English Channel, endolithic infestation may provide hosts with much
504 higher fitness than non-infested mussels. In fact, following a mass mortality event during a
505 relatively moderate heat wave (Seuront *et al.* 2019), the great majority (96% to 100%) of
506 empty mussel shells found on the shore had no sign of endolithic infestation (Seuront,
507 unpublished data). Therefore, in environments lacking topographic complexity, the
508 sustainability of intertidal mussel beds may increasingly depend on the thermal buffering
509 provided by endoliths. On the other hand, endolithic infestation comes with a series of costs
510 which can strongly reduce mussel fitness (e.g., weakening and fracturing of the shell, and
511 reduction of growth and reproductive output due to a shift in resources allocation for shell
512 repair) and can be responsible for a high proportion (> 50%) of total mortality, depending on
513 the severity of infestation (Kaehler & McQuaid 1999; Zardi *et al.* 2009; Marquet *et al.* 2013;
514 Ndhlovu, McQuaid & Monaco 2020). Given the costs imposed by endoliths, it seems unlikely
515 that these partners will enter a novel co-evolutionary pathway toward an entirely
516 mutualistic relationship. Nevertheless, most mutualistic relationships may have arisen from
517 successive evolutionary transitions which originated from an interaction with damaging
518 parasites that turned out to be beneficial under certain circumstances (Fellous & Salvaudon
519 2009). Although rare, other examples of parasites providing context-dependent advantages
520 do exist: some parasitic trematodes make marine snails more heat- and acidification-
521 tolerant (Bates *et al.* 2011; MacLeod & Poulin 2016) and some parasitic bacteria provide a
522 paramecium with protection against osmotic stress (Duncan *et al.* 2010). Particularly
523 important for further studies would be the evaluation of the fitness of infested individuals
524 relative to non-infested ones across all environments and whether endoliths modify their

525 hosts' thermal tolerances, for instance by reducing the expression of heat-shock proteins
526 due to altered resource allocation. The resolution of this specific issue, though of ecological
527 relevance, lies well beyond the scope of the present study, and warrants the need for
528 further work to further decipher the role of endolithic infestation on the thermal ecology of
529 mussels.

530

531 **Improving body temperature predictions**

532 Our predictions of body temperature using meteorological data from a global climate
533 reanalysis were comparable to those obtained with data from nearby weather stations. This
534 holds great promises for the prediction of body temperatures of terrestrial ectotherms (or
535 intertidal ones during emersion) at ecologically relevant spatiotemporal scales, as we may
536 reasonably bypass the practical issues associated with weather stations (e.g., data gaps).
537 Nevertheless, although we could predict mussel body temperature during aerial exposure
538 with reasonable accuracy (roughly within 2-3.5°C in most cases; Table S5), there is scope for
539 improvement. For example, further experiments are needed to assess how body
540 temperature is affected by smaller-scale topographical effects (e.g., the shapes of the
541 mussel itself or nearby boulders). Future research may also be able to account for the
542 effects of mussel aggregation on microclimates, such as evaporative cooling due to gaping
543 behaviour (Nicastro *et al.* 2012) or conductive heat transfer within multi-layer mussel beds
544 (Mislan & Wethey 2015). Likewise, enhanced evaporative cooling in infested mussels due to
545 higher water retention potential of eroded shells (Gehman & Harley 2019) may be
546 important. Here, we calculated shell reflectivity based on measurements of reflectance
547 within 350-1100 nm of the solar spectrum while the radiation reaching the Earth's surface is

548 non-negligeable until at least 2000 nm (Smith *et al.* 2016). Measuring shell reflectance of
549 both infested and non-infested mussels using a full-spectrum reflectometer (at least within
550 350-2100 nm) could help to improve body temperature predictions during aerial exposure.
551 Fully characterising the physiological, ecological, and evolutionary consequences of
552 endolithic infestation in natural mussel populations will require accurate estimates of
553 submerged body temperatures and the prediction of body temperatures during complete
554 tidal cycles (i.e., including during high tides when mussels are submerged). There are two
555 reasons that could explain why we could not predict body temperatures during
556 submergence with reasonable accuracy. First, we drove the biophysical model with water
557 temperatures extracted from a climate reanalysis whereas temperatures recorded *in-situ*
558 with buoys placed at our study sites could have provided better results (Lathlean, Ayre &
559 Minchinton 2011). To overcome this, we must rely on future improvements of climate
560 models that will capture the complexity of near-shore environments better and thus provide
561 estimates more biologically meaningful for subtidal and intertidal organisms. Second, we
562 used predictions of tidal heights obtained from XTide at locations sometimes quite distant
563 from our study sites (within 2.34-72.2 km; Table S2), to distinguish between periods of
564 submergence or aerial exposure. This can be problematic because the actual tidal height can
565 vary locally due to the geomorphology of the coast, the influence of wind, waves, and
566 atmospheric pressure. Not accounting for such sources of variation between predicted and
567 realized tidal levels could have led us to misidentify the times when mussels were emerged
568 or submerged. To overcome this, one could follow (i) Gilman *et al.* (2006) in accounting for
569 wave action when estimating mussel height on the shore and (ii) Mislan *et al.* (2011) in
570 tracing periods of emergence and submergence or exposure to surge and splash with water-
571 level loggers combined with temperature loggers.

572 Nevertheless, our main focus here was to evaluate thermal buffering due to differences in
573 shell reflectance, and this is mostly driven by solar radiation (Zardi *et al.* 2021), that is, when
574 mussels are exposed to terrestrial conditions. Our main conclusion that the moderating
575 effects of endoliths on body temperatures are greatest when and where temperatures are
576 most extreme will not be affected by predictions of body temperatures during
577 submergence.

578

579 ## References

580 Arribas, L.P., Donnarumma, L., Palomo, M.G. & Scrosati, R.A. (2014) Intertidal mussels as
581 ecosystem engineers: their associated invertebrate biodiversity under contrasting
582 wave exposures. *Mar. Biodiv.,* **44,** 203–211.
583 Bates, A.E., Leiterer, F., Wiedeback, M.L. & Poulin, R. (2011) Parasitized snails take the heat:
584 a case of host manipulation? *Oecologia,* **167,** 613–621.
585 Chamberlain, S. (2021) rnoaa: 'NOAA' Weather Data from R. R package version 1.3.2.
586 Cho, W.-J. & Kwon, S. (2010) Estimation of the thermal properties for partially saturated
587 granite. *Engineering Geology,* **115,** 132-138.
588 Cho, W.J., S. Kwon & Choi, J.W. (2009) The thermal conductivity for granite with various
589 water contents. *Engineering Geology,* **107,** 167–171.
590 Choi, F., Gouhier, T., Lima, F., Rilov, G., Seabra, R. & Helmuth, B. (2019) Mapping physiology:
591 biophysical mechanisms define scales of climate change impacts. *Conserv. Physiol.,* **7,**
592 coz028.

593 Clusella-Trullas, S., Terblanche, J.S., Blackburn, T.M. & Chown, S.L. (2008) Testing the
594 thermal melanism hypothesis: a macrophysiological approach. *Funct. Ecol.,* **22,** 232–
595 238.
596 Clusella Trullas, S., van Wyk, J.H. & Spotila, J.R. (2007) Thermal melanism in ectotherms. *J.*
597 *Therm. Biol.,* **32,** 235-245.
598 Denny, M.W., Dowd, W.W., Bilir, L. & Mach, K.J. (2011) Spreading the risk: Small-scale body
599 temperature variation among intertidal organisms and its implications for species
600 persistence. *J. Exp. Mar. Biol. Ecol.,* **400,** 175–190.
601 Di Lorenzo, E. & Mantua, N. (2016) Multi-year persistence of the 2014/15 North Pacific
602 marine heatwave. *Nat. Clim. Change,* **6,** 1042–1047.
603 Duffy, J.P. (in prep) mcera5: Tools to acquire and process ERA5 data for use in microclimate
604 modelling.
605 Duncan, A.B., Fellous, S., Accot, R., Alart, M., Sobandi, K.C., Cosiaux, A. & Kaltz, O. (2010)
606 Parasite-mediated protection against osmotic stress for *Paramecium caudatum*
607 infected by *Holospora undulata* is host genotype specific. *FEMS Microbiol. Ecol.,* **74,**
608 353–360.
609 Fellous, S. & Salvaudon, L. (2009) How can your parasites become your allies? *Trends*
610 *Parasitol.,* **25,** 62–66.
611 Geen, M.R.S. & Johnston, G.R. (2014) Coloration affects heating and cooling in three
612 colormorphs of the Australian bluetongue lizard, *Tiliqua scincoides*. *J. Therm. Biol.,*
613 **43,** 54–60.
614 Gehman, A.-L.M. & Harley, C.D.G. (2019) Symbiotic endolithic microbes alter host
615 morphology and reduce host vulnerability to high environmental temperatures.
616 *Ecosphere,* **10,** e02683.

Gibert, P., Moreteau, B., Moreteau, J.C., Parkash, R. & David, J.R. (1998) Light body pigmentation in Indian *Drosophila melanogaster*: a likely adaptation to a hot and arid climate. *J. Genet.,* **77,** 13–20.

Gilman, S.E., Harley, C.D.G., Strickland, D.C., Vanderstraeten, O., O'Donnell, M.J. & Helmuth, B. (2006) Evaluation of effective shore level as a method of characterizing intertidal wave exposure regimes. *Limnol. Oceanogr. Methods,* **4,** 448–445.

Gleason, F.H., Gadd, G.M., Pitt, J.I. & Larkum, A.W.D. (2017) The roles of endolithic fungi in bioerosion and disease in marine ecosystems. I. General concepts. *Mycology,* **8,** 205-215.

Golubic, S., Radtke, G. & Campion-Alsumard, T.L. (2005) Endolithic fungi in marine ecosystems. *Trends Microbiol.,* **13,** 229-235.

Gueymard, C.A. (2001) Parameterized transmittance model for direct beam and circumsolar spectral irradiance. *Solar Energy,* **71,** 325-346.

Harbach, H. & Palm, H.W. (2018) Development of general condition and flesh water content of long-time starved *Mytilus edulis*-like under experimental conditions. *Aquac. Aquar. Conserv. Legis.,* **11,** 301-308.

Harley, C.D.G. (2008) Tidal dynamics, topographic orientation, and temperature-mediated mass mortalities on rocky shores. *Mar. Ecol. Prog. Ser.,* **371,** 37–46.

Harley, C.D.G. & Helmuth, B.S.T. (2003) Local- and regional-scale effects of wave exposure, thermal stress, and absolute versus effective shore level on patterns of intertidal zonation. *Limnol. Oceanogr.,* **48,** 1498–1508.

Helmuth, B., Broitman, B.R., Blanchette, C.A., Gilman, S., Halpin, P., Harley, C.D.G., O'donnell, M.J., Hofmann, G.E., Menge, B. & Strickland, D. (2006) Mosaic patterns of

thermal stress in the rocky intertidal zone: implications for climate change. *Ecol. Monogr.,* **76,** 461–479.

Helmuth, B., Yamane, L., Lalwani, S., Matzelle, A., Tockstein, A. & Gao, N. (2011) Hidden signals of climate change in intertidal ecosystems: what (not) to expect when you are expecting. *J. Exp. Mar. Biol. Ecol.,* **400,** 191–199.

Helmuth, B.S.T. (1998) Intertidal mussel microclimates: predicting the body temperature of a sessile invertebrate. *Ecol. Monogr.,* **68,** 51–74.

Hersbach, H., Bell, B., Berrisford, P., Horányi, A., Sabater, J.M., Nicolas, J., Radu, R., Schepers, D., Simmons, A., Soci, C. & Dee, D. (2019) Global reanalysis: goodbye ERA-Interim, hello ERA5. *ECMWF Newsletter,* **159,** 17-24.

Hollister, J.W. (2020) elevatr: Access Elevation Data from Various APIs. R package version 0.3.1.

Hughes, T.P., Kerry, J.T., Álvarez-Noriega, M., Álvarez-Romero, J.G., Anderson, K.D., Baird, A.H., Babcock, R.C., Beger, M., Bellwood, D.R., Berkelmans, R., Bridge, T.C., Butler, I.R., Byrne, M., Cantin, N.E., Comeau, S., Connolly, S.R., Cumming, G.S., Dalton, S.J., Diaz-Pulido, G., Eakin, C.M., Figueira, W.F., Gilmour, J.P., Harrison, H.B., Heron, S.F., Hoey, A.S., Hobbs, J.-P.A., Hoogenboom, M.O., Kennedy, E.V., Kuo, C.-y., Lough, J.M., Lowe, R.J., Liu, G., McCulloch, M.T., Malcolm, H.A., McWilliam, M.J., Pandolfi, J.M., Pears, R.J., Pratchett, M.S., Schoepf, V., Simpson, T., Skirving, W.J., Sommer, B., Torda, G., Wachenfeld, D.R., Willis, B.L. & Wilson, S.K. (2017) Global warming and recurrent mass bleaching of corals. *Nature,* **543,** 373-377.

Judge, R., Choi, F. & Helmuth, B. (2018) Recent Advances in Data Logging for Intertidal Ecology. *Frontiers in Ecology and Evolution,* **6,** 213.

663 Kaehler, S. (1999) Incidence and distribution of phototrophic shell-degrading endoliths of
664 the brown mussel *Perna perna*. *Mar. Biol.,* **135,** 505-514.
665 Kaehler, S. & McQuaid, C.D. (1999) Lethal and sub-lethal effects of phototrophic endoliths
666 attacking the shell of the intertidal mussel *Perna perna*. *Mar. Biol.,* **135,** 497-503.
667 Kanamitsu, M., Ebisuzaki, W., Woollen, J., Yang, S.K., Hnilo, J.J., Fiorino, M. & Potter, G.L.
668 (2002) NCEP–DOE AMIP-II REANALYSIS (R-2). *Bulletin of the American Meteorological*
669 *Society,* **83,** 1631-1644.
670 Kearney, M. (2021) NicheMapR: R implementation of Niche Mapper software for biophysical
671 modelling. R package version 3.0.0.
672 Kearney, M.R., Gillingham, P.K., Bramer, I., Duffy, J.P. & Maclean, I.M.D. (2020) A method for
673 computing hourly, historical, terrain-corrected microclimate anywhere on earth.
674 *Methods Ecol. Evol.,* **11,** 38–43.
675 Kearney, M.R. & Porter, W.P. (2017) NicheMapR – an R package for biophysical modelling:
676 the microclimate model. *Ecography,* **40,** 664-674.
677 Kearney, M.R., Shamakhy, A., Tingley, R., Karoly, D.J., Hoffmann, A.A., Briggs, P.R. & Porter,
678 W.P. (2014) Microclimate modelling at macro scales: a test of a general microclimate
679 model integrated with gridded continental-scale soil and weather data. *Methods*
680 *Ecol. Evol.,* **5,** 273–286.
681 Kemp, M.U., van Loon, E.E., Shamoun-Baranes, J. & Bouten, W. (2012) RNCEP: global
682 weather and climate data at your fingertips. *Methods in Ecology and Evolution,* **3,** 65-
683 70.
684 Koepke, P., Hess, M., Schult, I. & Shettle, E.P. (1997) Global Aerosol Data Set. *Max-Planck-*
685 *Institut für Meteorologie, Hamburg,* **Report No. 243**.

686 Kwon, S., Kim, J.S., Lee, C.S. & Cho, W.J. (2011) The thermal and mechanical properties rock
687 mass around an underground research tunnel in granite body. *Harmonising Rock*
688 *Engineering and the Environment* (eds Q. Qian & Y. Zhou), pp. 2048 pp. CRC Press,
689 London.
690 Lathlean, J.A., Ayre, D.J. & Minchinton, T.E. (2011) Rocky intertidal temperature variability
691 along the southeast coast of Australia: comparing data from *in situ* loggers, satellite-
692 derived SST and terrestrial weather stations. *Mar. Ecol. Prog. Ser.,* **439,** 83–95.
693 Le Nohaïc, M., Ross, C.L., Cornwall, C.E., Comeau, S., Lowe, R., McCulloch, M.T. & Schoepf, V.
694 (2017) Marine heatwave causes unprecedented regional mass bleaching of thermally
695 resistant corals in northwestern Australia. *Sci. Rep.,* **7,** 14999.
696 Maclean, I.M.D., Mosedale, J.R. & Bennie, J.J. (2018) Microclima: An R package for modelling
697 meso-and microclimate. *Methods Ecol. Evol.,* **10,** 280–290.
698 MacLeod, C.D. & Poulin, R. (2016) Parasitic infection: a buffer against ocean acidification?
699 *Biol. Lett.,* **12,** 20160007.
700 Marquet, N., Nicastro, K.R., Gektidis, M., McQuaid, C.D., Pearson, G.A., Serrão, E.A. & Zardi,
701 G.I. (2013) Comparison of phototrophic shell-degrading endoliths in invasive and
702 native populations of the intertidal mussel *Mytilus galloprovincialis*. *Biol. Invasions,*
703 **15,** 1253–1272.
704 Mateparae, K.M. (2003) Optimisation of the Thermal Processing of Mussels. Master of
705 Technology, Massey University.
706 McKechnie, A.E. & Wolf, B.O. (2010) Climate change increases the likelihood of catastrophic
707 avian mortality events during extreme heat waves. *Biol. Lett.,* **6,** 253–256.
708 Meehl, G.A. & Tebaldi, C. (2004) More Intense, More Frequent, and Longer Lasting Heat
709 Waves in the 21st Century. *Science,* **305,** 994-997.

Met Office (2019a) MIDAS Open: UK hourly rainfall data, v201908. *Centre for Environmental Data Analysis, 30 October 2019*.

Met Office (2019b) MIDAS Open: UK hourly solar radiation data, v201908. *Centre for Environmental Data Analysis, 30 October 2019*.

Met Office (2019c) MIDAS Open: UK hourly weather observation data, v201908. *Centre for Environmental Data Analysis, 30 October 2019*.

Mislan, K.A.S., Blanchette, C.A., Broitman, B.R. & Washburn, L. (2011) Spatial variability of emergence, splash, surge, and submergence in wave-exposed rocky-shore ecosystems. *Limnology and Oceanography,* **56,** 857–866.

Mislan, K.A.S. & Wethey, D.S. (2015) A biophysical basis for patchy mortality during heat waves. *Ecology,* **96,** 902-907.

Monaco, C.J. & McQuaid, C.D. (2018) Applicability of Dynamic Energy Budget (DEB) models across steep environmental gradients. *Scientific Reports,* **8,** 16384.

Monaco, C.J., Wethey, D.S. & Helmuth, B. (2016) Thermal sensitivity and the role of behavior in driving an intertidal predator–prey interaction. *Ecological Monographs,* **86,** 429-447.

Monsinjon, J.R., McQuaid, C.D., Nicastro, K.R., Seuront, L., Oróstica, M.H. & Zardi, G.I. (2021) Data from: Weather and topography regulate the benefit of a conditionally helpful parasite. Dryad Digital Repository.

Mosedale, J., Bennie, J. & Duffy, J. (2021) microclima: microclimate modelling with R. R package version 0.1.0.

Ndhlovu, A., McQuaid, C.D. & Monaco, C.J. (2020) Ectoparasites reduce scope for growth in a rocky-shore mussel (*Perna perna*) by raising maintenance costs. *Sci. Total Environ.,* **753,** 142020.

734 Nicastro, K.R., Zardi, G.I., McQuaid, C.D., Pearson, G.A. & Serrão, E.A. (2012) Love Thy
735 Neighbour: Group Properties of Gaping Behaviour in Mussel Aggregations. *PLoS One,*
736 **7,** e47382.
737 Oliver, E.C.J., Donat, M.G., Burrows, M.T., Moore, P.J., Smale, D.A., Alexander, L.V.,
738 Benthuysen, J.A., Feng, M., Gupta, A.S., Hobday, A.J., Holbrook, N.J., Perkins-
739 Kirkpatrick, S.E., Scannell, H.A., Straub, S.C. & Wernberg, T. (2018) Longer and more
740 frequent marine heatwaves over the past century. *Nat. Commun.,* **9,** 1324.
741 Porter, W.P. & Gates, D.M. (1969) Thermodynamic Equilibria of Animals with Environment.
742 *Ecol. Monogr.,* **39,** 227-244.
743 Porter, W.P., Mitchell, J.W., Beckman, W.A. & DeWitt, C.B. (1973) Behavioral implications of
744 mechanistic ecology: Thermal and behavioral modeling of desert ectotherms and
745 their microenvironment. *Oecologia,* **13,** 1–54.
746 Pruvot, M., Cappelle, J., Furey, N., Hul, V., Heng, H.S., Duong, V., Dussart, P. & Horwood, P.
747 (2019) Extreme temperature event and mass mortality of insectivorous bats. *Eur. J.*
748 *Wildl. Res.,* **65,** 41.
749 R Core Team (2021) R: A language and environment for statistical computing. R Foundation
750 for Statistical Computing, Vienna, Austria.
751 Rouxel, M., Ruiz, L., Molénat, J., Hamon, Y., Chirié, G. & Michot, D. (2012) Experimental
752 Determination of Hydrodynamic Properties of Weathered Granite. *Vadose Zone*
753 *Journal,* **11,** vzj2011.0076.
754 Sanford, E. & Kelly, M.W. (2011) Local Adaptation in Marine Invertebrates. *Annual Review of*
755 *Marine Science,* **3,** 509-535
756 Schneider, T., Kaul, C.M. & Pressel, K.G. (2019) Possible climate transitions from breakup of
757 stratocumulus decks under greenhouse warming. *Nat. Geosci.,* **12,** 163–167.

758 Seabra, R., Wethey, D.S., Santos, A.M. & Lima, F.P. (2011) Side matters: Microhabitat
759 influence on intertidal heat stress over a large geographical scale. *J. Exp. Mar. Biol.*
760 *Ecol.,* **400,** 200–208.
761 Seuront, L., Nicastro, K.R., Zardi, G.I. & Goberville, E. (2019) Decreased thermal tolerance
762 under recurrent heat stress conditions explains summer mass mortality of the blue
763 mussel *Mytilus edulis*. *Sci. Rep.,* **9,** 17498.
764 Smale, D.A. (2020) Impacts of ocean warming on kelp forest ecosystems. *New Phytol.,* **225,**
765 1447–1454.
766 Smale, D.A., Wernberg, T., Oliver, E.C.J., Thomsen, M., Harvey, B.P., Straub, S.C., Burrows,
767 M.T., Alexander, L.V., Benthuysen, J.A., Donat, M.G., Feng, M., Hobday, A.J.,
768 Holbrook, N.J., Perkins-Kirkpatrick, S.E., Scannell, H.A., Gupta, A.S., Payne, B.L. &
769 Moore, P.J. (2019) Marine heatwaves threaten global biodiversity and the provision
770 of ecosystem services. *Nat. Clim. Change,* **9,** 306–312.
771 Smith, K.R., Cadena, V., Endler, J.A., Porter, W.P., Kearney, M.R. & Stuart-Fox, D. (2016)
772 Colour change on different body regions provides thermal and signalling advantages
773 in bearded dragon lizards. *Proc. R. Soc. B,* **283,** 20160626.
774 Somero, G.N. (2010) The physiology of climate change: how potentials for acclimatization
775 and genetic adaptation will determine 'winners' and 'losers'. *J. Exp. Biol.,* **213,** 912-
776 920.
777 Sorte, C.J.B., Bernatchez, G., Mislan, K.A.S., Pandori, L.L.M., Silbiger, N.J. & Wallingford, P.D.
778 (2019) Thermal tolerance limits as indicators of current and future intertidal
779 zonation patterns in a diverse mussel guild. *Mar. Biol.,* **166,** 6.
780 Thyrring, J., Tremblay, R. & Sejr, M.K. (2019) Local cold adaption increases the thermal
781 window of temperate mussels in the Arctic. *Conservation Physiology,* **7,** coz098.

782 Turner, J. & Lombard, A. (1990) Body color and body temperature in white and black Namib
783 desert beetles. *J. Arid Environ.,* **19,** 303–315.
784 Umbers, K.D.L., Herberstein, M.E. & Madin, J.S. (2013) Colour in insect thermoregulation:
785 Empirical and theoretical tests in the colour-changing grasshopper, *Kosciuscola*
786 *tristis*. *J. Insect Physiol.,* **59,** 81–90.
787 Walsberg, G.E. (1983) Coat color and solar heat gain in animals. *Bioscience,* **33,** 88-91.
788 Walsberg, G.E., Campbell, G.S. & King, J.R. (1978) Animal coat color and radiative heat gain:
789 A re-evaluation. *J. Comp. Physiol. B,* **126,** 211-222.
790 Welbergen, J.A., Klose, S.M., Markus, N. & Eby, P. (2008) Climate change and the effects of
791 temperature extremes on Australian flying-foxes. *Proc. R. Soc. B,* **275,** 419–425.
792 Wellborn, G.A. & Langerhans, R.B. (2015) Ecological opportunity and the adaptive
793 diversification of lineages. *Ecol. Evol.,* **5,** 176–195.
794 Zardi, G.I., Monsinjon, J.R., McQuaid, C.D., Seuront, L., Oróstica, M.H., Want, A., Firth, L.B. &
795 Nicastro, K.R. (2021) Foul-weather friends: Modelling thermal stress mitigation by
796 symbiotic endolithic microbes in a changing environment. *Global Change Biology,* **27,**
797 2549-2560.
798 Zardi, G.I., Nicastro, K.R., McQuaid, C.D. & Gektidis, M. (2009) Effects of Endolithic
799 Parasitism on Invasive and Indigenous Mussels in a Variable Physical Environment.
800 *PLoS One,* **4,** e6560.
801 Zardi, G.I., Nicastro, K.R., McQuaid, C.D., Ng, T.P.T., Lathlean, J. & Seuront, L. (2016) Enemies
802 with benefits: parasitic endoliths protect mussels against heat stress. *Sci. Rep.,* **6,**
803 31413.
804 Zeileis, A. & Grothendieck, G. (2005) zoo: S3 Infrastructure for Regular and Irregular Time
805 Series. *Journal of Statistical Software,* **14,** 1–27.

Acknowledgements

This work is based upon research supported by the National Research Foundation of South Africa (Grant number 64801). The work was also financially supported by a Pierre Hubert Curien PESSOA Program, projects UIDB/04326/2020 from the Fundação para a Ciência e Tecnologia (FCT-MEC, Portugal), and by Rhodes University.

Conflict of interest

The authors declare no conflict of interest.

Authors' contributions

JRM initiated the project and conducted the data analysis. JRM conceived the manuscript with contributions from CDM, GIZ and KRN. GIZ, KRN, MO, and LS collected field data. JRM wrote the manuscript with contributions from all authors.

Data availability

Robomussel data are available from the Dryad Digital Repository: https://doi.org/10.5061/dryad.79cnp5hwg (Monsinjon *et al.* 2021).

Code availability

The modelling code used in the present study is available upon reasonable request from the corresponding author.

Supporting information

Additional supporting information may be found in the online version of this article.

826 FEMonsinjonSF1to7&ST1to5.docx [Supplementary Material (Figures S1-7 and Tables S1-5)]

Commenté [JM4]: pdf